GDFIDL WITH GENERALIZED DIAGONAL FILLINGS AND PERIODIC BOUNDARY CONDITIONS

W. Bruns*, Technische Universität Berlin, EN-2, Berlin, Germany

Abstract

GdfidL is a code that computes resonant electromagnetic fields and time dependent fields. It uses the Finite Difference approximations of the curl operators as introduced by Yee in 1966. GdfidL uses generalized diagonal fillings for the discretization of the material distribution. The new algorithm allows more than 72 different types of material filling for each cell, whereas the common diagonal filling only allows 7 types. With the improved material filling, the discretization error is reduced by a factor of ten. The improved meshing is implemented both in the resonant solver and the time domain solver. The implementation of the generalized diagonal fillings is described. Computed frequencies for a sphere are given to show the reduction in discretization error.

For resonant fields, GdfidL allows periodic boundary conditions in all three cartesian directions simultaneously. It is shown that, although periodic boundary conditions lead to an eigenvalue problem with a complex matrix, the matrix iterations can be carried out mostly in real arithmetic. As an example for the application of periodic boundary conditions, the dispersion relation of some artificial crystal is computed.

1 INTRODUCTION

The Finite Difference algorithm for electromagnetic fields replaces MAXWELL's curl equations by difference equations. The coefficients of the difference equations depend both on the grid-spacing and on the material parameters.

Of course, generally the solution of the difference equations differ from the solution of the differential equations. We have at least two sources of error:

- The error introduced by the approximation of the differential equation by a difference equation. For a homogeneous mesh, this error is proportional to the square of the mesh spacing.

- The error due to the approximation of the material distribution.

In order to achieve a good result from our field computations, we have to keep both errors low. The most economical case is when both errors are of about the same size.

We describe a procedure that decreases the error due to the approximation of the material filling down to a level comparable to the error due to the difference equation itself.

---

*bruns@tetibm2.ee.TU-Berlin.DE

2 IMPROVED MESH FILLING

The coefficients of the difference equations do depend on the material parameters. The simplest finite difference programs assume constant material parameters in each cell of the grid. This is the "staircase" approximation. A better approximation of the material fillings can be achieved with prismatic cells, as e.g. the MAFIA [5] group of codes uses them. The filling with prismatic cells can be generalized. Since the finite difference coefficients for a field component depend only on the material in the immediate vicinity of the edge where the component is defined on, one can work easily with a mesh-filling that is constructed by a boolean combination of prismatic fillings. Figure 1 shows some of the possible discretized material distributions. A similiar mesh filling is mentioned in [3].
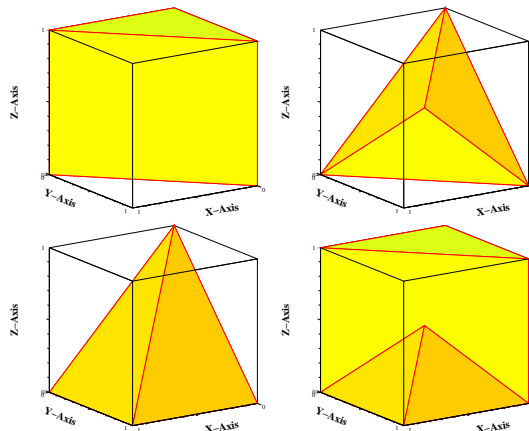

Figure 1: Some examples of the possible inhomogeneous fillings of a cell. Upper left: a prism. lower left: Intersection of two prisms. Upper right: Intersection of three prisms. lower right: Union of "upper left" and "lower left". The prism in the upper left can be oriented in 2 x 3 different kinds in a cell, the other three material fillings are possible in 4 x 3 x 2 different orientations.

2.1 Effect of the new meshing

In order to show the effect of the generalized prismatic filling, figure 2 shows the computed resonance frequency in a sphere as a function of the mesh-spacing. For comparison, the results for prismatic filling and the optimal quadratic behaviour is plotted also. The error with the improved filling is about as low as the optimal quadratic behaviour. If the boundary conditions, ie. the materials would have been discretized perfectly, the result would not be much better.
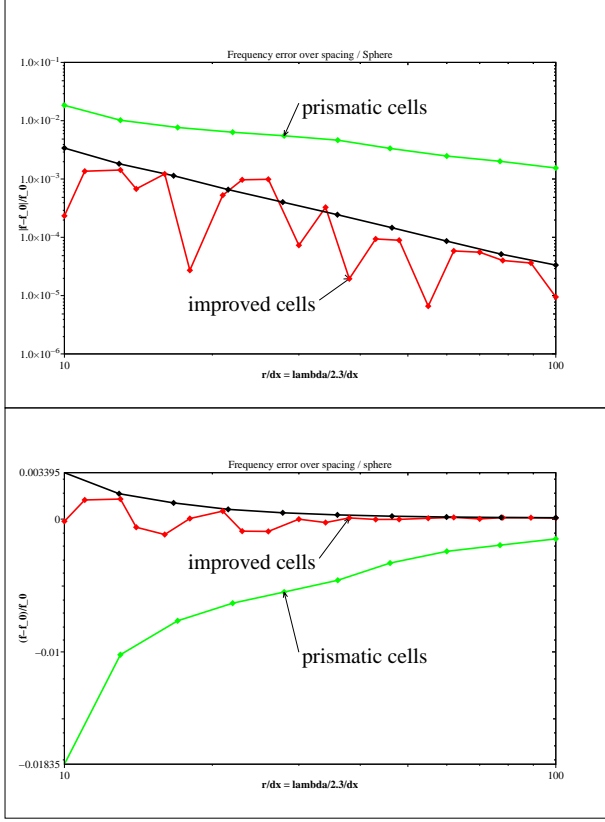
Figure 2: Error in the computed frequency of the lowest mode in a sphere. Above: absolute values in a double logarithmic scale, below: signed values in single logarithmic scale.

2.2 Difference equations

The Finite Difference algorithm substitutes MAXWELL's curl equations by difference equations for the line integrals $\int \vec{E} \cdot d\vec{s}$ and $\int \vec{H} \cdot d\vec{s}$ along discrete edges $\Delta \vec{s}$.

The derivation of our difference coefficients is strongly influenced by the works of Weiland, who calls the procedure "Finite Integration Theory" [4]. The derivation of the finite difference coefficients starts from FARADAYs and AMPEREs laws in lossfree regions:

$$-\frac{d}{dt} \int_A \mu \vec{H} \cdot d\vec{A} = \oint_{\delta A} \vec{E} \cdot d\vec{s} \quad (1)$$

$$\frac{d}{dt} \int_{A'} \varepsilon \vec{E} \cdot d\vec{A}' = \oint_{\delta A'} \vec{H} \cdot d\vec{s}' \quad (2)$$

In the Finite Integration Algorithm, the areas we integrate over are the faces A of the primary grid or the faces A' of the dual grid. This is the same grid as it was introduced by Yee [1]. When the material boundaries are just tangential or normal to these faces, we can assume average field strengths over these faces: We extract the field strengths out of the surface integrals:

$$-\int_A \mu dA \frac{d}{dt} \vec{H} \cdot \vec{n}_A \approx \oint_{\delta A} \vec{E} \cdot d\vec{s} \quad (3)$$

$$\int_{A'} \varepsilon dA' \frac{d}{dt} \vec{E} \cdot \vec{n}_{A'} \approx \oint_{\delta A'} \vec{H} \cdot d\vec{s}' \quad (4)$$

The line integrals on the right sides of the above equations are sums of four line integrals along the edges of the primary and dual grid, respectively. In order to have such line integrals on the left sides too, we now integrate these equations over the edges of the primary or dual grid.

$$-\frac{d}{dt} \int \vec{H} \cdot d\vec{s}' \approx \int \frac{\oint_{\delta A} \vec{E} \cdot d\vec{s}}{\int_A \mu dA} ds \quad (5)$$

$$\frac{d}{dt} \int \vec{E} \cdot d\vec{s} \approx \int \frac{\oint_{\delta A'} \vec{H} \cdot d\vec{s}'}{\int_{A'} \varepsilon dA'} ds \quad (6)$$

Assuming that the contour integrals on the right sides are spatially constant, we arrive at:

$$-\frac{d}{dt} \int \vec{H} \cdot d\vec{s}' \approx \int \frac{1}{\int_A \mu dA} ds \oint_{\delta A} \vec{E} \cdot d\vec{s} \quad (7)$$

$$\frac{d}{dt} \int \vec{E} \cdot d\vec{s} \approx \int \frac{1}{\int_{A'} \varepsilon dA'} ds \oint_{\delta A'} \vec{H} \cdot d\vec{s}' \quad (8)$$

Our unknowns are now the line integrals of the fields along the edges of the primary and dual cells. With $e \approx \int \vec{E} \cdot d\vec{s}$ and $h \approx \int \vec{H} \cdot d\vec{s}$, we can drop the approximation signs and write

$$-\frac{d}{dt} h = \int \frac{1}{\int_A \mu dA} ds' (e_1 + e_2 - e_3 - e_4) \quad (9)$$

$$\frac{d}{dt} e = \int \frac{1}{\int_{A'} \varepsilon dA'} ds (h_1 + h_2 - h_3 - h_4) (10)$$

The values $\int \frac{1}{\int_{A'} \varepsilon dA'} ds$ and $\int \frac{1}{\int_A \mu dA} ds'$ are the coefficients of the difference equations. The values h_i and e_i are the line integrals of the field strengths surrounding the component on the left side of the equations.

2.3 Computing the FD-Coefficients

GdfidL further approximates the FD-coefficients by assuming for the coefficients $\int \frac{1}{\int_{A'} \varepsilon dA'} ds$ that the value $\int_{A'} \varepsilon dA'$ is constant over the integration path Δs. Therefore GdfidL uses an FD-coefficient of $\frac{\int ds}{\int_{A'} \varepsilon dA'}$. The area where the permittivity has to be integrated over is the vicinity of an edge of the primary grid. Four cells belong to this vicinity. In the case of the implemented generalized diagonal fillings, each cell can have up to two different materials. Figure 3 illustrates the case that all material boundaries in the four cells involved also touch the edge. The integral $\int_{A'} \varepsilon dA'$ in the FD-coefficient now is

$$\left. \begin{array}{l} \int_{A'} \varepsilon dA' = \frac{1}{8} \big((\varepsilon_{1,1} + \varepsilon_{2,1}) A_1 + (\varepsilon_{1,2} + \varepsilon_{2,2}) A_2 \\ + (\varepsilon_{1,3} + \varepsilon_{2,3}) A_3 + (\varepsilon_{1,4} + \varepsilon_{2,4}) A_4 \big) \end{array} \right\} \quad (11)$$

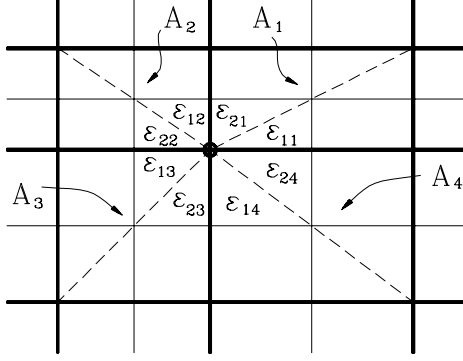The value $\int ds$ of course is the length of the edge of the primary grid.

Figure 3: The FD-coefficients to compute an electric component from the surrounding magnetic components are dependent on up to eight different permittivities. The marker in the above picture indicates the location of the electric component. The areas A_1, A_2, A_3, A_4 are the areas of faces of the primary grid cells touching the edge where the electric component is defined on. The thick lines indicate edges of the primary grid, the thin lines indicate edges of the dual grid.

To evaluate the coefficient of a magnetic component $\int \frac{1}{\int_A \mu dA} ds'$, we integrate the permeability in the vicinity of a dual edge. Since a dual edge is the connection of the two centers of two primary cells, the dual edge lies within two primary cells. GdfidL assumes that in each primary cell the integral $\int_A \mu dA$ does not change along the part of the dual edge inside the cell. Since in each primary cell up to two different materials may be present, the FD-coefficient for a magnetic component then may be calculated as:

$$\int \frac{1}{\int_A \mu dA} ds' = \frac{1}{2}\left(\frac{\Delta_1}{(\mu_{1,1}+\mu_{2,1})A_1/2} \right. \\ \left. + \frac{\Delta_2}{(\mu_{1,2}+\mu_{2,2})A_2/2} \right) \quad (12)$$

Here the values $\mu_{1,1}, \mu_{2,1}$ and $\mu_{1,2}, \mu_{2,2}$ are the material parameters in the two primary cells involved, and the values $A_1 = A_2$ are the areas of their faces.

Figure 4 illustrates the material distribution in one of the two primary cells involved. Figure 5 illustrates a common case that a magnetic field component is tangential to a material boundary.

3 EIGENVALUE COMPUTATION

Equations (9) and (10) may be written as matrix equations for arithmetic vectors $\vec{e}$ and $\vec{h}$ which hold the unknown integrated electric and magnetic field strengths over the primary and dual edges:

$$-\frac{d}{dt}\vec{h} = (C)^e \vec{e} \quad (13)$$

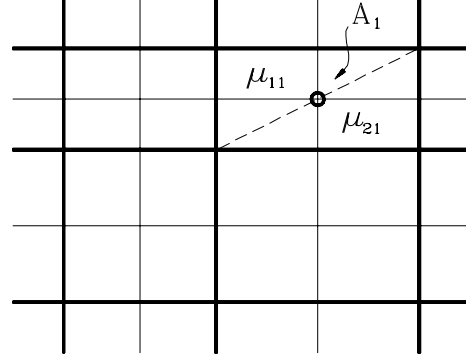$$\frac{d}{dt}\vec{e} = (C)^h \vec{h} \quad (14)$$

Figure 4: The marker in the above picture indicates the location of the magnetic component. The FD-coefficients to compute a magnetic component from the surrounding electric components are dependent of up to four different permeabilities. Two of the permeabilities involved are the permeabilities in the shown cell, the other two permeabilities belong to the cell above the paper plane. The thick lines indicate edges of the primary grid, the thin lines indicate edges of the dual grid.
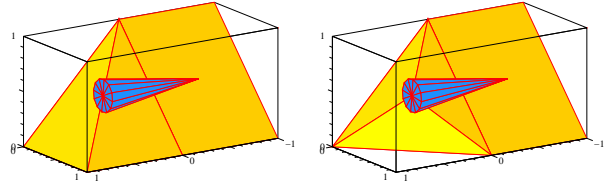

Figure 5: A magnetic field component touching some material boundaries. To evaluate the FD-coefficient for this component, one has to evaluate the effectice permeability along the path where the component is defined on. The Finite Difference coefficient for *this* component is the same in both shown cases.

Here the elements of the matrix $(C)^e$ are $\pm \int \frac{1}{\int_A \mu dA} ds'$ and the elements of the matrix $(C)^h$ are $\pm \int \frac{1}{\int_{A'} \varepsilon dA'} ds$. The matrices are extremely sparse, there are only up to 4 nonzero entries per row. If we would want to perform a FDTD computation, then we would perform a FDTD-step with these matrices as:

$$\vec{h}_n = \vec{h}_{n-1} - \Delta t (C)^e \vec{e}_{n-1/2} \quad (15)$$

$$\vec{e}_{n+1/2} = \vec{e}_{n-1/2} + \Delta t (C)^h \vec{h}_n \quad (16)$$

Since we want to compute resonant fields, we can substitute $j\omega$ for $\frac{d}{dt}$. Substituting the $\vec{h}$ of equation (13) into (14) yields a standard arithmetic eigenvalue problem:

$$(C)^h (C)^e \vec{e} = \omega^2 \vec{e} \quad (17)$$

If the boundary conditions at the outer boundaries of the computational volume are simple ones, ie. if the outer boundaries can be assumed perfectly electric conducting or perfectly magnetic conducting, then the matrix of the eigenvalue problem $(C)^h (C)^e$ is real.

If we want to compute eigenvalues with periodic boundary conditions applied at the outer surface of our computational volume, then some of the matrix elements become complex, since the periodic boundary conditions specify that eg. the electric field at a lower boundary has to be the same as the field at the corresponding upper boundary, multiplied with a complex factor $e^{-\mathrm{j}\varphi}$.

GdfidL uses subspace iteration as implemented in an algorithm of Tückmantel [2] to search for the lowest nonzero eigenvalues of (17). This algorithm needs some hundred to some thousand iterations of the form:

$$\vec{y}_{i+1} = (C)^h (C)^e \vec{y}_i - \gamma_i \vec{y}_i \qquad (18)$$

where the γ_i are the zeroes of some polynomial. Since the algorithm only requires these matrix times vector operations, and not the matrix itself, it is not necessary to really construct and store the matrix.

For periodic boundary conditions, GdfidL implements the matrix times vector operation (18) in a four step process, without performing a complex matrix times vector operation. Two of these steps are very similar to the operations needed to perform a single time step in a FDTD algorithm. In order to avoid the computation with a complex matrix, GdfidL extends the grid such, that above the last gridplane of the computational volume an auxiliary plane with the same material distribution as the very first plane is placed. Below the lowest plane of the computational volume, an auxiliary plane with the same material distribution as the last plane is placed. This is done for all cartesian directions where periodic boundary conditions are to be enforced.

In the first step, a complex auxiliary vector $\vec{x}$ is computed.

$$\vec{x} <= (C')^e \vec{y}_i \qquad (19)$$

Here the entries of the real matrix $(C')^e$ are the real FD-coefficients $\pm \int \frac{1}{\int \mu dA} ds$ in the artificially enlarged volume. If the vector $\vec{y}_i$ would contain the integrated electric field strengths of a resonant field with frequency ω_n, then this auxiliary vector $\vec{x}$ would be the integrated magnetic field strengths of $\mathrm{j}\omega_n \vec{H}$. This step is similiar to the computation of the H-field update in an FDTD-algorithm. To compute this auxiliary vector, it is not needed to store the matrix $(C')^e$, it is only needed to be able to perform a H-field update.

In the second step, the periodic boundary conditions for the H-fields are applied to the complex auxiliary vector $\vec{x}$. This is: The components of $\vec{x}$ that lie at the lower boundaries of the computational volume are multiplied by a complex factor $\psi = \exp(\mathrm{j}\varphi)$ and the result is copied to the corresponding components at the upper planes. Here φ is the wanted phase shift for the cartesian direction. Figure 6 illustrates this procedure for a 2-dimensional grid, when periodic boundary conditions in a single cartesian direction are to be enforced.

In the third step, the vector update

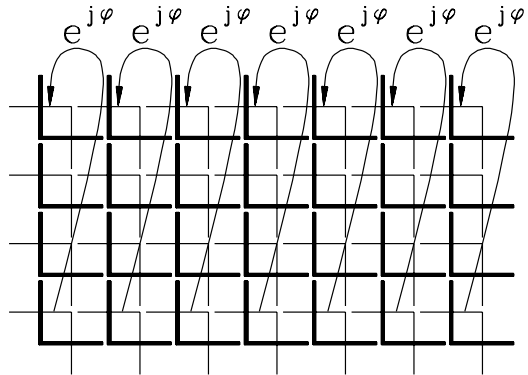$$\vec{y}_{i+1} <= (C')^h \vec{x} - \gamma_i \vec{y}_i \qquad (20)$$

Figure 6: The periodic boundary conditions for the magnetic field are enforced by taking the values at the lower plane, multiplying them by a complex factor and assigning the result to the magnetic field components at the upper plane. The thick lines indicate edges of the primary grid, the thin lines indicate edges of the dual grid.

is performed. Here the entries of the real matrix $(C')^h$ are the real FD-coefficients $\pm \int \frac{1}{\int \varepsilon dA'} ds$ in the artificially enlarged volume. This step is similiar to the E-field update in a FDTD-algorithm. Again, the matrix $(C')^h$ does not need to be explicitly available.

In the fourth step, the periodic boundary conditions for the electric field are applied to the vector $\vec{y}_{i+1}$. This is: The components of $\vec{y}_{i+1}$ that lie at the upper boundaries of the computational volumes are multiplied by a complex factor $\psi = \exp(-\mathrm{j}\varphi)$ and the results are copied to the corresponding components at the lower planes. Again φ is the wanted phase shift for the cartesian direction. Figure 7 illustrates this procedure for a 2-dimensional grid, when periodic boundary conditions in a single cartesian direction are to be enforced.
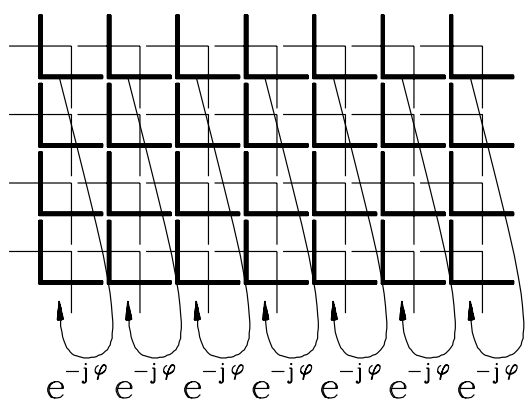

Figure 7: The periodic boundary conditions for the electric field are enforced by taking the values at the upper plane, multiplying them by a complex factor and assigning the result to the electric field components at the lower plane. The thick lines indicate edges of the primary grid, the thin lines indicate edges of the dual grid.

3.1   Example for Periodic Boundary Conditions

The periodic boundary conditions are applied to compute the dispersion relation in a crystal made of a rectangular array of conducting spheres connected by round rods. Figure 8 shows an elemental cell of this array. This geometry also is a nice example for the good material approximation that can be achieved with the generalized diagonal fillings. Figure 9 shows the computed frequencies as a function of the wave-vector $\vec{k}$.
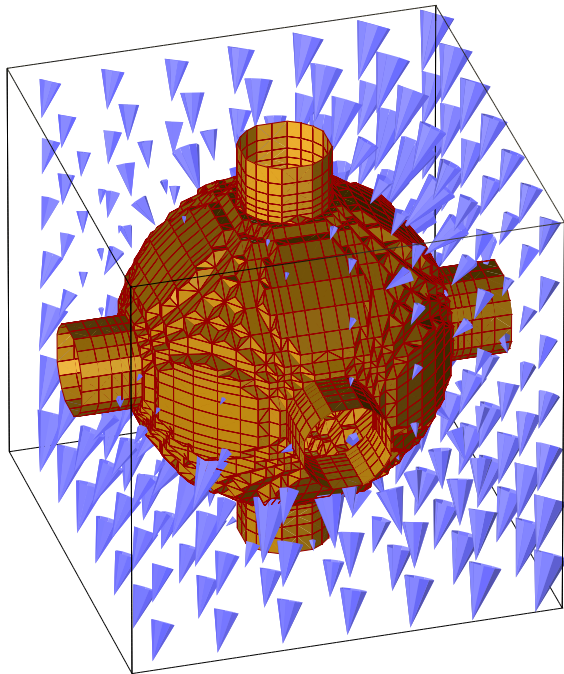

Figure 8: The elemental cell of a 3D array of perfect conducting spheres, connected by round conducting rods. The lattice constant a is the same in all three directions, the radius of the spheres is $0.375\,a$, the radius of the rods is $a/10$. The spheres are located at $(x, y, z) = (la, ma, na)$, $(l, m, n \in \cdots -2, -1, 0, 1, 2, 3 \cdots)$. The shown field is the real part of the fundamental mode with $\vec{k} = (1, 1, 1)\frac{\pi}{4a}$.
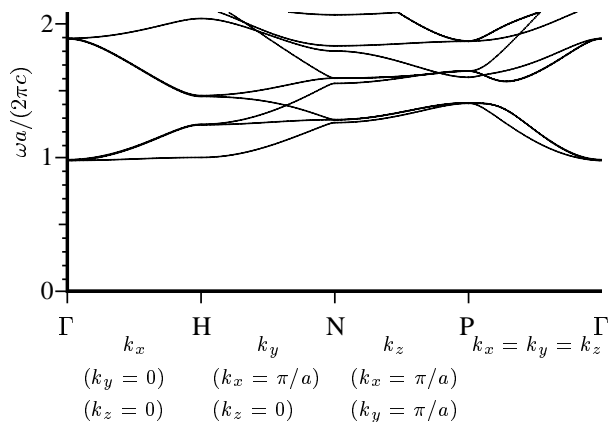

Figure 9: The band structure for the first few modes in the 3D array.

4   CONCLUSION

An improved mesh filling has been described that reduces the frequency error by a factor of ten as compared to a prismatic filling. The described mesh filling can be used both for time domain computations and eigenvalue computations. The procedure to evaluate the Finite Difference coefficients with this material approximation has been described in detail.

Periodic boundary conditions for all three cartesian directions simultaneously can be applied to eigenvalue problems without having to build a complex matrix. Instead only procedures similiar to the ones needed to perform a FDTD step are needed.

5   REFERENCES

[1] Kane S. Yee, "Numerical solution of initial boundary value problems involving Maxwell's equations in isotropic media", *IEEE Transactions on Antennas and Propagation*, vol. 14, May 1966

[2] J. Tückmantel, "An improved version of the eigenvector processor SAP applied in URMEL", CERN/EF/RF 85-4, 4 July 1985

[3] W. Müller, J. Krueger, A. Jacobus. R. Winz, T. Weiland, H. Euler, U. Hamm, W. R. Novender, "Numerical Solution of 2- or 3-Dimensional Nonlinear Field Problems by Means of the Computer Program PROFI", *Archiv für Elektrotechnik 65* (1982) pp. 299-307

[4] T. Weiland, "On the numerical solution of Maxwell's equations and applications in the field of accelerator physics", *Particle Accelerators*, vol. 15, pp. 245-292, 1984

[5] F. Ebeling, R. Klatt, F. Krawczyk, E. Lawinsky, T. Weiland, S. G. Wipf, B. Steffen, T. Barts, M. J. Browman, R. K. Cooper, H. Deaven, G. Rodenz, "The 3-D MAFIA group of electromagnetic codes", *IEEE Transactions on Magnetics*, vol. 25, pp. 2962-2964, July 1989